Astron. Astrophys. 355, 1060–1072 (2000)

ASTRONOMY AND ASTROPHYSICS

The effective temperature scale of giant stars (F0-K5)

III. Stellar radii and the calibration of convection

A. Alonso[1], **M. Salaris**[2], **S. Arribas**[1], **C. Martínez-Roger**[1], **and A. Asensio Ramos**[1]

[1] Instituto de Astrofísica de Canarias, E-38200 La Laguna, Tenerife, Spain (aas@ll.iac.es; sam@ll.iac.es; cmr@ll.iac.es; aasensio@ll.iac.es)
[2] Astrophysics Research Institute, Liverpool John Moores University, Twelve Quays House, Egerton Wharf, Birkenhead CH41 1LD, UK (ms@staru1.livjm.ac.uk)

Received 17 November 1999 / Accepted 22 December 1999

Abstract. We present an analysis of radii of giant stars with 6200 K$\geq T_{\rm eff} \geq$ 3800 K based on angular diameters obtained by means of the IRFM and distances computed from Hipparcos parallaxes. In order to asses the reliability of IRFM diameters we have considered a selected sample of stars whose diameters have been directly measured by interferometric techniques with internal errors below 5%. The intercomparison shows a fairly good consistency and no systematic differences against temperature are apparent in the analysis. By averaging the individual values obtained for a sample of approximately 300 stars, we present mean values of linear radii of giants of solar metallicity; the results are tentatively extended to metal-poor giants.
We have also devised a method to derive distance moduli of globular clusters complementary to the standard Main Sequence (MS) and Horizontal Branch (HB) fitting. This method is based on the fit of observed linear radii and effective temperatures of Red Giant Branch stars of a given globular cluster to the yields of theoretical isochrones. A careful assessment of the uncertainty on the derived distances is provided. As expected, the distances are critically dependent on the value of the mixing length parameter adopted in the stellar models. We have applied the method to provide a homogeneous distance scale for a representative sample of Galactic globular clusters. The comparison of these distances with the distance scale obtained by means of the MS- or HB-fitting permits a consistent calibration and/or test of the superadiabatic gradient in stellar envelopes, independent of the use of colour-$T_{\rm eff}$ transformations.

Key words: convection – stars: fundamental parameters – stars: Population II – stars: general – stars: distances – Galaxy: globular clusters: general

1. Introduction

Radius (R), together with mass (M) and luminosity (L), is a fundamental parameter which characterizes the equilibrium configuration of a stationary star. Therefore, the observational values of R for individual stars are useful to set constraints to the theory of stellar structure and evolution. In particular, they are basic to understand the nature of the stars which populate the Red Giant Branch (RGB) of the HR diagram.
The determination of linear stellar radii requires the measurement of both distances and angular diameters. Angular diameters can be directly determined by means of interferometric techniques. Distances to stars are determined by measuring the trigonometric parallax. In practice, accurate linear radii determined from direct measurements of the above quantities are scarce for two reasons. On the one hand, interferometric techniques with internal precision better than 5% are restricted so far to bright stars. On the other, the measurement of trigonometric parallaxes with comparable precision is limited to nearby stars. Before the measurements carried out with the Hipparcos satellite, the precision attainable in the linear radii was rather poor even for nearby stars. The recent release of the parallaxes measured with Hipparcos (ESA 1997) has had the effect of increasing the precision with which linear radii can now be determined. This fact has in turn intensified the efforts devoted to extend the mesurements of accurate angular diameters in the range 2–20 milliarcseconds (e.g. Dick et al. 1998, van Belle et al. 1999). In spite of these efforts, a considerable fraction of nearby stars which have now an accurate parallax are too faint as to permit a direct measurement of their angular diameters by conventional interferometric techniques. In the absence of direct angular diameters, those indirectly estimated by means of the InfraRed Flux Method (Blackwell et al. 1990; IRFM) are a good remedy in order to increase the accuracy of linear radii of population I stars, and also allow to extend their determination to metal-poor stars.

In a previous paper (Alonso et al. 1999; Paper I) we have presented effective temperatures and bolometric fluxes for a large sample of giant stars representative of the different populations of the Galaxy. Here, we derive angular diameters which are then combined with the Hipparcos parallaxes in order to obtain stellar linear radii. Furthermore, the data obtained in Paper I for stars on the RGB of a sample of Globular Clusters (GCs) allow the implementation of a new method to estimate their distance moduli. The method is based on the comparison of IRFM angular diameters and temperatures with the yields of theoretical

Send offprint requests to: A. Alonso

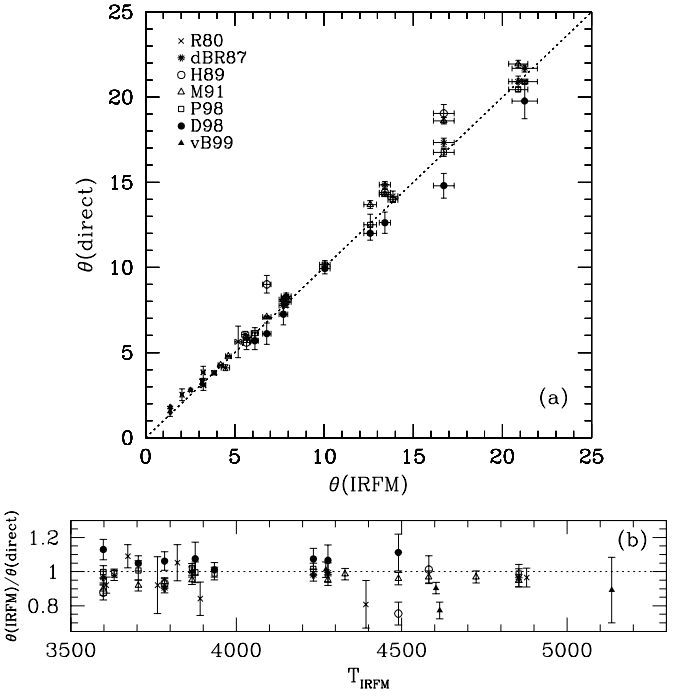

Fig. 1. Comparison between angular radii derived by means of the IRFM and those directly measured by lunar occulation or Michelson interferometry. Symbols stand for the following references: R80 Ridgway et al. (1980); dBR87 Di Benedetto and Rabbia (1987); H89 Hutter et al. (1989); D98 Dick et al. (1998); P98 Perrin et al. (1998); vB99 van Belle et al. (1999).

isochrones in the plane $T_{\rm eff}$: R. The comparison between the results obtained with this method and the distances from MS- or HB-fitting provides a rigorous way for calibrating the mixing length in Population II stars.

The paper is laid as follows. In Sect. 2, as a preliminary step prior to the use of parallaxes, we show the consistency of IRFM angular diameters with those directly measured. Then, we derive mean linear radii of population I and II giants based on a sample of approximately 300 field stars, with IRFM angular diameters and Hipparcos parallaxes. The results are compared with those of other authors.

In Sect. 3, we describe a new method devised to derive distance moduli of a sample of Galactic globular clusters, and compare the results with those obtained from MS- and HB-fitting, in order to calibrate the efficiency of convection.

We summarize the results in Sect. 4.

2. Radii of giant stars

2.1. Angular diameters

In principle stellar angular diameters can be directly measured by means of interferometric observations. Angular diameters resolved with present interferometric devices are roughly distributed in the range 2–20 *milliarcseconds*. The internal accuracy of these measurements typically ranges from 1 to 10% (e.g. Mozurkewich et al. 1991).

In the absence of a direct measurement, angular diameters can be indirectly determined by considering the basic equation:

$$\frac{\theta}{2} = \left[\frac{F_{\rm Bol}}{\sigma T_{\rm eff}^4}\right]^{1/2}, \quad (1)$$

where $F_{\rm Bol}$ is the bolometric flux measured at the top of the earth's atmosphere, σ is the Stefan-Boltzmann constant and $T_{\rm eff}$ is the effective temperature of the star. The angular radius ($\theta/2$), defined through Eq. (1) corresponds to the so–called intensity (angular) radius which is comparable to (angular) radii directly measured (see Baschek et al. 1991). The internal accuracy of the indirect determinations can be estimated through:

$$\epsilon(\theta) = \frac{1}{2}\epsilon(F_{\rm Bol}) + 2\epsilon(T_{\rm eff}), \quad (2)$$

where $\epsilon(F_{\rm Bol})$ and $\epsilon(T_{\rm eff})$ stand, respectively, for the estimated errors of bolometric flux and temperature. Considering that, typically, mean internal errors of the bolometric fluxes ($F_{\rm Bol}$) are around 2% and errors on $T_{\rm eff}$ range 1–3%, then accidental errors of θ range 2–7%.

The level of the internal errors of direct and indirect determinations of angular diameters is hence comparable. However, in order to properly understand the results of the comparison one must take also into account typical systematic errors which could affect both methods. On the one hand, systematic differences observed between different temperature scales range 1-3%, and those in fluxes range 3–5%, hence the expected systematic discrepancies might reach at most 10% for indirect diameters. On the other hand, in the case of direct measurements, the combined effects of particular systematic errors associated to each method (e.g changes in visibility amplitude caused by scintillation in Michelson interferometry, or nonuniformities of the lunar limb in Lunar occultations), and also limb-darkening corrections, although difficult to quantify, result in a level of systematic errors also of the order of 5-10%. In summary, when comparing homogeneus sets of values of direct and indirect diameters and taking into account accidental and systematic errors, one should expect that the mean differences were smaller than 5-15%, with a dispersion within the range 3-12%. This a priori estimation is in good agreement with results obtained below (Table 1 and Fig. 1).

In order to support the above analysis, a natural question must be raised at this point: Are θ derived by means of the IRFM comparable to those directly measured? Baschek et al. (1991) present a thorough discussion of the different stellar radii usually used in astrophysics. They conclude that for stars with compact atmospheres (this denomination excludes late M giants, nuclei of planetary nebulae and Wolf–Rayet stars) all type of stellar radii defined (i.e. intensity radius, Rosseland radius, etc) practically coincide. Hence for the giants contained in our sample which roughly cover F0 to K5 types with a minimal presence of late K and early M stars, $\theta_{\rm IRFM}$ are directly comparable to $\theta_{\rm direct}$ obtained with interferometric techniques provided the latter are corrected for limb darkening.

Table 1. Comparison between the angular diameters derived by means of the IRFM (Column 3) and those derived by *direct* methods (Columns 4). Units are milliarcseconds.

Star	$T_{\rm IRFM}$ (K)	$\theta_{\rm IRFM}$	$\theta_{\rm direct}$
HR 165	4329±53	4.20±0.13	4.12±0.04[f]
HR 168	4582±60	5.66±0.19	5.64±0.05[f], 5.4±0.4[g]
HR 337	3783±29	13.41±0.31	12.2±0.6[b], 14.35±0.19[d], 13.81±0.13[f], 13.9±0.2[g]
HR 603	4277±50	7.72±0.24	7.0±0.6[b], 7.50±0.36[d], 7.84±0.07[f]
HR 617	4490±61	6.79±0.23	5.9±0.6[b], 6.85±0.07[f], 8.7±0.5[g]
HR 911	3704±39	12.59±0.36	12.08±0.6[a], 11.6±0.4[b], 13.23±0.22[f]
HR 1457	3866±35	20.89±0.53	19.75±0.11[a], 20.21±0.30[d], 21.21±0.21[f]
HR 2012	4604±43	2.52±0.07	2.79±0.06[c]
HR 2286	3631±23	13.86±0.28	13.50±0.15[a], 13.7±0.3[e]
HR 2938	3822±65	3.24±0.13	2.97±0.29[e]
HR 2990	4854±68	7.88±0.28	7.70±0.30[a], 7.90±0.31[d], 8.04±0.08[f]
HR 4432	3891±41	3.23±0.09	3.71±0.35[e]
HR 4902	3607±52	5.58±0.20	5.85±0.18[e]
HR 5301	3672±82	4.48±0.23	3.97±0.17[e]
HR 5340	4233±55	21.25±0.72	20.20±0.08[a], 19.1±1.0[b], 20.95±0.20[d]
HR 5429	4271±53	3.84±0.12	3.80±0.12[c]
HR 5824	4392±57	2.04±0.07	2.44±0.33[e]
HR 6705	3934±42	10.05±0.29	9.82±0.23[a], 9.6±0.3[b]
HR 7635	3867±50	6.12±0.20	5.94±0.30[a], 5.5±0.5[b]
HR 7776	4878±55	3.18±0.10	3.18±0.15[e]
HR 7949	4725±62	4.63±0.16	4.62±0.04[f]
HR 7995	5135±74	1.37±0.05	1.54±0.29[c]
HR 8775	3598±49	16.72±0.58	16.19±0.23[a], 14.3±0.7[b], 16.75±0.24[d], 17.98±0.18[f], 18.4±0.5[g]
HR 8834	3762±51	5.19±0.18	5.44±0.89[e]
HR 8930	4615±53	1.38±0.05	1.79±0.07[c]

[a] Perrin et al. (1998); [b] Dick et al. (1998); [c] van Belle et al. (1999); [d] Di Benedetto & Rabbia. (1987); [e] Ridgway et al. (1980); [f] Mozurkewich et al. (1991); [g] Hutter et al. (1989).

2.1.1. Comparison between $\theta_{\rm direct}$ and $\theta_{\rm IRFM}$

In addition to the theoretical result by Baschek et al. (1991), we present in this section the observational evidences for the consistency of interferometric diameters with those derived by means of the IRFM. For this purpose we have considered all the stars in the sample which have recent measurements of their angular diameter by interferometry with an internal accuracy $\lesssim 5\%$. There are basically two sources of measurements of red giant stars angular diameters with internal accuracies around this level: Lunar occultation techniques and Michelson interferometry. In Table 1, we present 25 stars whose diameters have been measured with either of the mentioned methods. This subsample serves to illustrate the reliability of the IRFM angular diameters, since it covers a wide range in temperature. The comparison between angular diameters derived from the IRFM and those directly measured are shown in Fig. 1. If one adopts a conservative criterion of 2 standard deviations of difference, it is worth noticing the fairly good agreement in general. This is a consequence of the absolute calibration of the flux adopted to implement the IRFM (Alonso et al. 1994) which was derived by minimizing differences $(\theta_{\rm IRFM}-\theta_{\rm direct})$. However for a certain number of stars, IRFM diameters disagree by more than 3 standard deviations with direct diameters. This is a clear symptom of the presence of systematic errors which exceed accidental ones. Two major sources of possible errors have to be noticed: First, the limb–darkening correction applied to interferometric measurements may bias the inferred angular diameters, feigning even a spurious wavelength dependence of the corrected diameters (Baschek et al 1991). Furthermore, the possible presence of circumstelar dust shells absorbing and scattering energy radiated by stars may cause greater apparent diameters as measured by direct techniques. Limb-darkening correction has obviously no effect on the θ derived by means of the IRFM, however the second effect quoted above may influence the yields of the IRFM, the diminution of the bolometric and monochromatic flux measured would cause a $\theta_{\rm IRFM}$ greater than the actual one (the size of this effect is difficult to estimate).

In any case, we can safely conclude that no correction of the angular diameters derived by means of the IRFM seems to be necessary in order to match the direct scale of angular diameters.

2.2. Linear radii of giant stars

Once obtained angular radii by using effective temperatures and bolometric fluxes, linear radii are easy to derive combining them

with distances based on trigonometric parallaxes, through the basic equation:

$$R = \theta \, \frac{D}{2}, \tag{3}$$

where D is the parallactic distance. Temperatures and bolometric fluxes have been derived for approximately 300 giant stars (Paper I) whose parallaxes have been measured by Hipparcos satellite. Typical errors of Hipparcos parallaxes range from 2% to 20% for the stars of our sample. In consequence, taking into account the expected errors in $\theta_{\rm IRFM}$ (3-7%), errors in the derived linear radii should range 5–27%. These errorbars when considered for an individual star are discouragingly large, however by grouping stars in temperature bins and obtaining mean values, it is possible to limit the effect of the errors of parallaxes on the derived average $R/R_{\odot}$. We have computed mean radii by grouping stars within bins 200 K in size, with an step of 100 K beginning at 3600 K. The selected bin size corresponds roughly to the mean errors of the IRFM temperatures. We have checked that no significant variations occured when changing slightly the sizes of the bin and the step. From a theoretical point of view, a smooth and gradual change of radii is to be expected for the stars contained in the short range of temperatures considered in each group, however different factors may alter this fact: (1) accidental errors on parallaxes, temperatures and bolometric fluxes, (2) contamination of the sample with unresolved binary, multiple stars or stars from luminosty classes other than III, and/or (3) true internal variation due to metal content, age, etc. Before averaging values, we have rejected stars departing significantly from the smooth mean trend in each bin; the reason for the occurrence of these outliers can be probably ascribed to point (2). Nevertheless a considerable scatter of radii of individual stars around the mean line remains as a consequence of points (1) and (3). A reasonable evaluation of the internal error on the radius for each temperature bin may be obtained by considering that the differences around the mean value are approximately gaussian, so that the standard error of the mean is a good estimate (i.e. $\epsilon = \sigma/\sqrt{(n)}$ where n is the number of stars contained in the bin). Unfortunately in a number of the bins, specially in the range $3.72 < log(T_{\rm eff}) < 3.76$ (which roughly corresponds to the so-called Hertzsprung gap), the number of stars in our sample is too small as to provide significant error estimates.

The possible systematic errors in the temperatures and/or the bolometric fluxes has an effect on the radii which can be estimated having into account Eq. (1). If we consider a zero-point error of 2% in the temperatures and 3% in the bolometric fluxes, then, the net effect of these systematic uncertainties is a drift of the radii scale. If it happens that the above errors correlate (both positive or negative), the maximum possible variation of the radii scale would amount to $\pm$2.5%. However, if the systematic errors in temperature and bolometric fluxes are uncorrelated, the shift of the radii would amount to at most $\pm$5.5%.

In Table 2 we present the empirical mean radii, distances and temperatures obtained for stars with $[Fe/H] \geq -0.5$. The variation with temperature of the mean stellar radii obtained is displayed in Fig. 2; notice that mean distances are around 200 parsecs. In the ranges, $log(T_{\rm eff}) > 3.71$ (subgiant stars) and $log(T_{\rm eff}) < 3.67$ (RGB stars) the observed behaviour of the mean trend of radii with effective temperature shows a remarkable agreement with theoretical predictions of evolutionary models. In Fig. 2, we show models for [Fe/H]=–0.35 and [Fe/H]=0.0, homogeneous with the ones discussed in the following sections. However, in the range $3.71 > log(T_{\rm eff}) > 3.67$, it is worth noticing that the mean observed behaviour slightly departs from theoretical predictions. Theoretical isochrones predict a smooth growth of radii with effective temperature. The empirical radii show a plateau in the range $3.71 > log(T_{\rm eff}) > 3.67$, at constant radii larger than those predicted from theoretical isochrones (although still within the error-bars). Since the observed sample of stars is composed of a mixture of metallicites and ages, this fact might well explain such a minor discrepancy. In Fig. 3, we show the comparison of the present results with those obtained by van Belle et al. (1999), as it can be seen the agreement is fairly good.

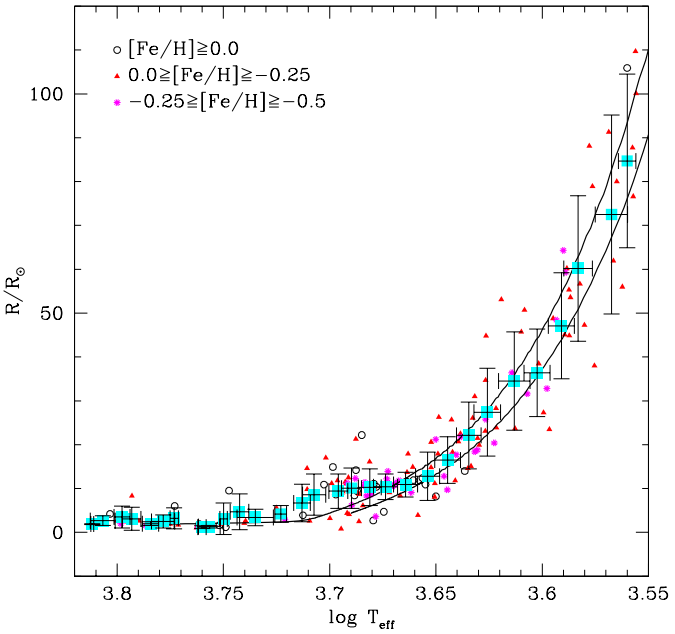

Fig. 2. Mean stellar radii for $[Fe/H] \geq -0.5$ (squares). The small symbols correspond to the individual stars considered in the averages, separated in metallicity groups. A theoretical isochrone of the RGB with [Fe/H]=0 and $t = 3.5$ Gyr, and another of the RGB and Subgiant branch with [Fe/H]=–0.35 and $t = 4.5$ Gyr are overimposed for comparison.

In Table 3 we show the results obtained for stars with $[Fe/H] \leq -0.75$. Once age, Y and $(l/H_{\rm p})$ are fixed, if we consider a grid of isochrones in the HR diagram, for a given temperature the more metal-poor a giant star the larger its luminosity and radius (Notice that in the case of dwarf stars it is just the contrary, metal-poor dwarf stars are subluminous and have smaller radii). This is due to the fact that a decrease in the metallicity decreases the opacity in the stellar envelope, which completely determines the effective temperature of RGB stars,

Table 2. Linear radii derived for the stars of the sample with $[Fe/H] \geq -0.5$. Cols 1–2: Mean effective temperatures in K and corresponding standard deviation. Col 3–4: Mean distances in parsecs and corresponding standard deviation. Col 5–6: Mean radii in solar units with standard deviation. Cols 7-8: Mean metallicity with standard deviation. Col 8: Number of stars in the bin.

$T_{\rm eff}$	$\sigma(T_{\rm eff})$	D	$\sigma(D)$	$R/R_\odot$	$\sigma(R/R_\odot)$	$[Fe/H]$	$\sigma([Fe/H])$	n
3631	34	148	67	84.7	19.8	0.0	0.1	8
3693	65	124	71	72.5	22.7	0.0	0.1	11
3829	59	126	67	60.2	16.6	-0.1	0.2	13
3899	55	165	130	47.1	12.1	-0.1	0.2	15
4003	57	227	228	36.4	10.0	-0.2	0.2	12
4103	70	199	208	34.5	11.2	-0.2	0.2	11
4225	61	123	71	27.4	10.0	-0.2	0.2	17
4310	57	109	72	22.1	7.6	-0.2	0.2	21
4410	62	85	54	16.5	5.3	-0.2	0.2	22
4507	58	75	62	12.8	5.5	-0.2	0.2	19
4616	60	70	54	10.9	2.8	-0.2	0.2	22
4717	62	81	57	10.4	2.9	-0.2	0.2	33
4798	59	83	63	10.3	4.2	-0.2	0.2	34
4894	53	69	47	10.1	4.6	-0.1	0.2	31
4965	51	61	39	9.4	3.9	-0.1	0.2	20
5097	64	52	28	8.6	4.7	-0.1	0.2	11
5164	47	50	14	6.7	4.3	-0.2	0.2	7
5285	–	53	–	4.2	–	-0.2	–	2
5432	107	43	22	3.4	1.9	0.0	0.0	3
5526	55	53	37	4.7	4.1	0.0	0.1	3
5622	23	57	45	3.1	3.6	-0.1	0.3	5
5709	67	39	30	1.3	0.3	-0.1	0.2	11
5755	26	34	20	1.2	0.3	-0.1	0.2	7
5931	26	54	29	3.2	2.4	0.0	0.1	3
6003	75	40	22	2.5	1.5	-0.2	0.2	7
6085	54	36	18	2.0	0.4	-0.3	0.2	6
6211	62	46	22	3.1	2.6	-0.2	0.2	6
6276	54	48	19	3.5	2.5	-0.1	0.3	6
6408	87	47	11	2.7	1.1	0.0	0.3	4
6481	–	39	–	1.9	–	-0.1	–	2

and therefore the effective temperature increases at a fixed luminosity. Because of the steep slope of the RGB in the HR diagram, a metal poor star must reach a higher luminosity and radius for attaining the same effective temperature as a more metal rich one of the same age (in the case of dwarf stars, a lower metal content shifts evolutionary tracks toward higher effective temperatures as an effect of the lower opacity, but the slope of the MS in the HR diagram is opposite to the RGB one, so that, for a fixed $T_{\rm eff}$, the lower the metallicity the smaller the radius).
The above effect can be observed when comparing Fig. 2 with Fig. 4. Furthermore, the dispersion of the average radii is much greater than the corresponding quantity for metal-rich stars. In this case, a part of the dispersion is caused by the mixture of metallicities and ages, but also an important part is ascribed to internal uncertainties on radii caused by errors in parallaxes. Regarding this point, notice that mean distances for the metal-poor sample are over 300 parsecs. Overimposed in Fig. 4, we show the theoretical lines corresponding to isochrones of 9 Gyrs with [Fe/H]=–0.7 and 12 Gyrs with [Fe/H]=–2.3 (Salaris & Weiss 1998). Notice that considering the size of errorbars, empirical points are within the limits predicted by theory. In the range $log(T_{\rm eff}) < 3.66$, radii seem to be smaller than expected, however for cool giants below 4000 K, parallaxes and IRFM angular diameters are affected by large errors. Moreover, in the range $log(T_{\rm eff}) > 3.72$ it is appreciated that the plateau of the Subgiant Branch is reached at slightly lower temperatures and higher radii than theoretical isochrones. A similar behaviour was observed for Population I stars.

3. Distance of stellar clusters

The GCs in our Galaxy are too far from the solar neighbourhood as to permit an accurate measurement of their trigonometric parallax. For instance one of the nearest, M4, is 2.2 kpc from the sun and consequently would have a parallax of 0.0005 arcsec. That value is beyond the threshold of detectability of trigonometic parallaxes. Take into account that for stars fainter than $V \approx 9$ the mean error of the Hipparcos parallaxes is 0.001 arcsec, and therefore at 1 kpc the relative error in the distance becomes practically 100%!
In the absence of a direct measurement, two methods are used to derive globular cluster distances (Sandage 1986 provides a

Table 3. Linear radii derived for he stars of the sample with $[Fe/H] < -0.5$. Cols 1–2: Mean effective temperatures in K and corresponding standard deviation. Col 3–4: Mean distances in parsecs and corresponding standard deviation. Cols 5–6: Mean radii in solar units with standard deviation. Cols 7–8: Mean metallicity with standard deviation. Col 9: Number of stars in the bin.

$T_{\rm eff}$	$\sigma(T_{\rm eff})$	D	$\sigma(D)$	$R/R_\odot$	$\sigma(R/R_\odot)$	$[Fe/H]$	$\sigma([Fe/H])$	n
4158	99	666	489	37.0	33.0	-1.9	0.3	6
4261	53	483	277	31.1	15.5	-1.6	0.5	8
4302	72	460	272	31.2	14.0	-1.6	0.6	9
4443	68	518	561	23.3	13.0	-1.6	0.5	11
4521	73	541	523	21.5	11.3	-1.8	0.5	16
4619	71	718	604	21.2	12.8	-2.1	0.6	14
4734	79	715	583	17.9	15.4	-2.1	0.7	12
4850	65	424	395	9.8	9.1	-1.8	0.7	16
4927	77	398	360	10.6	8.8	-1.7	0.6	19
5020	68	442	266	10.5	5.4	-1.6	0.5	17
5117	80	450	298	8.8	4.5	-1.6	0.5	15
5226	59	442	366	7.1	4.9	-1.8	0.5	12
5291	56	370	320	6.6	4.6	-1.8	0.6	11
5399	62	487	201	8.2	3.3	-1.7	0.4	4
5567	72	281	205	5.3	4.6	-1.5	0.1	3
5654	61	286	290	5.6	5.2	-1.5	0.6	4
5676	51	280	355	4.1	5.3	-1.4	0.7	3
5866	197	554	192	7.6	3.7	-2.0	0.2	2
6049	62	434	23	6.0	1.3	-2.2	0.4	2
6131	149	313	211	4.4	2.8	-2.1	0.4	3

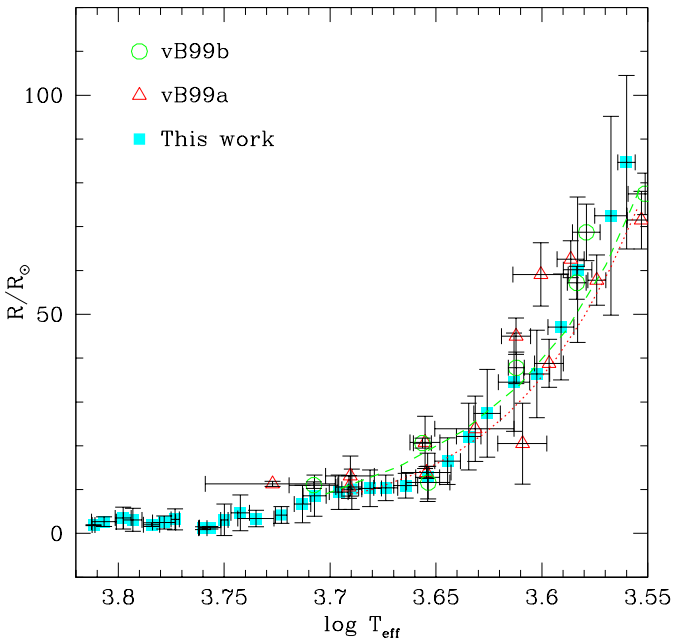

Fig. 3. Comparison between the values obtained in this work and those obtained by van Belle et al (1999) for solar metallicity stars. Circles: vB99 radii averaged by temperatures, the dashed line shows their mean fit to the data. Triangles: vB99 radii averaged by spectral types, the dotted line shows their mean fit to the data.

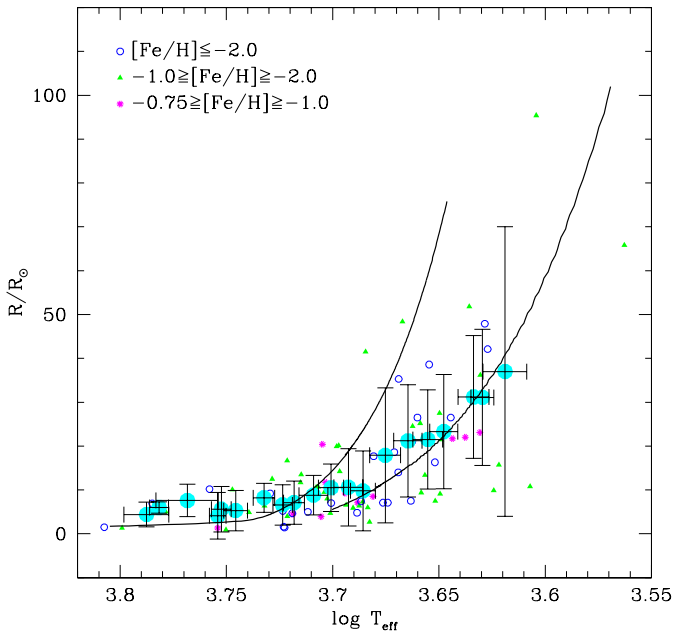

Fig. 4. Mean stellar radii of metal–poor stars (black circles). The small symbols correspond to the individual stars considered in the averages, separated in metallicity. A theoretical isochrone of the RGB with [Fe/H]=–0.7 and $t = 9$ Gyr, and another of the RGB and Subgiant branch with [Fe/H]=–2.3 and $t = 12$ Gyr are overimposed for comparison.

detailed account). The first one is based on the fit of observed colours and magnitudes of main sequence stars of GCs to the fiducial zero age main sequence of the corresponding metallicity (MS-fitting). The second one is based on the use of the $M_{\rm V}$-[Fe/H] relation for RR Lyrae stars in the clusters HB[1]. We

[1] Obviously, this method is not applicable if the cluster lacks variables.

will discuss here an alternative method to estimate GCs distances. It is based on the fitting of the observational relation $T_{\rm eff} - R$ for individual stars of the clusters RGB to the corresponding relation from theoretical isochrones (hereafter this method will be indistinctly referred to as RGB-fitting or $T_{\rm eff} - R$ method). The implementation of the method demands the *a priori* knowledge of age, metallicity, helium abundance, reddening and superadiabatic convection calibration.

Assuming fixed the calibration of convection, the present method, as compared to the MS- or HB-fitting, has the disadvantage of depending on age. From a theoretical standpoint there exists a small risk of vicious circle since the age is derived after deriving the cluster distance basically from the turn-off absolute brightness. However as it will be shown in the section below, a variation of 2-3 Gyrs would imply a maximum diference in radii smaller than the typical observational errors. For this reason, we can ensure that the method is, for practical purposes, weakly dependent on age.

Taking into account that the primary observable data used in the fit are θ and $T_{\rm eff}$, the fit in the plane $T_{\rm eff}$–R has an important advantage versus the fit in the plane $T_{\rm eff}$–L (or equivalently $T_{\rm eff}$–$M_{\rm bol}$). In the former, distance enters as the first power in the determination R from θ, in the latter as the second power in the determination of L, therefore the relative error in the distance as derived here is in principle decreased by a factor of 2.

However, we must face the problem of the superadiabatic convection in the envelope of RGB stars. The lack of a rigorous theory of convection remains one of the major deficiencies in the calculation of stellar evolutionary sequences. The mixing length theory by Böhm-Vitense (1958) is widely adopted (although there exist also alternative approaches see Canuto et al. 1996 and references therein); it involves the adjustable parameter $l/H_{\rm p}$, the ratio of the mixing-length to the pressure scale height, whose value affects the model radius and effective temperature, but leaves basically unaffected the luminosity. The value of this parameter is not predicted by the theory and must therefore be calibrated by comparison with empirical stellar radii and temperatures. The usual procedure consists of fixing $l/H_{\rm p}$ by reproducing the solar radius at the Sun age and luminosity, but there are no a priori reasons ensuring that the solar calibrated mixing length is suitable also for different evolutionary phases and/or metallicites. Recent 2-D radiation hydrodynamics simulations carried out by Ludwig et al. (1999), seem to support the fact that $l/H_{\rm p}$ value, at least in the MS and low RGB region of low mass stars, appears to vary by no more than $\sim \pm 0.05 - 0.10$ respect to the solar value, in the range of metallicities and ages typical of galactic GC (see also Freytag & Salaris 1999). Unfortunately, there are no theoretical indications about the behaviour of $l/H_{\rm p}$ along the rest of the RGB. In addition, the effective temperatures and radii of RGB stars are strongly affected by the mixing length and in general by the treatment of the superadiabatic gradient in the convective envelope.

In this respect, the comparison of the distances derived by using the MS- or HB-fitting techniques, which are unaffected by mixing length and cluster age, with the distances obtained from the RGB-fitting method, provides a useful technique for calibrating and/or testing the superadiabatic convection in low mass metal-poor stars of the RGB, independent of colour-$T_{\rm eff}$ transformations.

The use of clusters RGB stars for calibrating and testing the convection in Population II objects is a widely employed technique. Empirical $M_{\rm bol}$ and $T_{\rm eff}$ values determined by Frogel et al. (1981) for a sample of Galactic GC have been repeatedly used in the past for comparing the $T_{\rm eff}$ of theoretical RGB models with the average empirical $T_{\rm eff}$ determined at a given level of $M_{\rm bol}$ given a distance scale (e.g., Mazzitelli et al. 1995, Salaris & Cassisi 1996). Concerning this point we recall (paper I) that temperatures derived by means of the IRFM are $\sim$50 K smaller than those derived by Frogel et al. (1981); this shift would imply a variation of –0.1 in $l/H_{\rm p}$. In addition, differences in bolometric correction for giant stars ranges ± 0.10 mag; the corresponding variation in $M_{\rm bol}$ induces a change in effective temperature amounting to $\sim \pm 25$ K, therefore the effect on the calibration of $l/H_{\rm p}$ is around ± 0.05. In any case, by restricting the comparison to a single brightness level, as with the usual procedure, one is using only part of the available empirical information. The procedure proposed here takes advantage of the observed features of globular cluster RGBs in a somewhat efficient manner, and permits as well a careful and clear assessment of the errors involved in the fit.

In the following subsection we will discuss in detail the errors on the RGB-fitting distances due to the uncertainties in the input parameters of the models.

3.1. Theoretical relations $T_{\rm eff}$–R

In order to fit the observed $T_{\rm eff} - R$ values of RGB stars to theoretical predictions, we have considered the grid of theoretical isochrones computed by Salaris & Weiss (1998), extended to the tip of the RGB by Weiss & Salaris (1999). For a full description of the models the reader is referred to the mentioned papers. Here, we briefly recall that the models are computed employing the OPAL equation of state (Rogers et al. 1996), the effect of alpha-enhanced elements ($[\alpha/Fe] = 0.4$) has been properly taken into account in the burning as well as in the opacity tables (Alexander & Ferguson 1994, Iglesias & Rogers 1996), and the mixing length value has been fixed to the solar value $l/H_{\rm p} = 1.8$. Since the absolute value of $l/H_{\rm p}$ depends on the adopted mixing length formalism and boundary conditions for the stellar models, we mention that the Cox & Giuli (1968) formalism and the Krishna-Swamy (1966) $T(\tau)$ relation has been employed in the models.

The helium abundance follows the relation $Y = 0.23 + 3Z$, in agreement with the findings of Pagel & Portinari (1998). Nevertheless, we notice that the effect on RGB radii due to a variation of the helium abundance in the range 0.23–0.27 is practically negligible. Additional models, completely consistent with the Salaris & Weiss (1998) ones, have been computed for the solar metallicity cluster M67, but this time with a scaled solar heavy elements mixture. Morever, isochrones with different values of Y and $l/H_{\rm p}$ have been computed for testing the dependence of

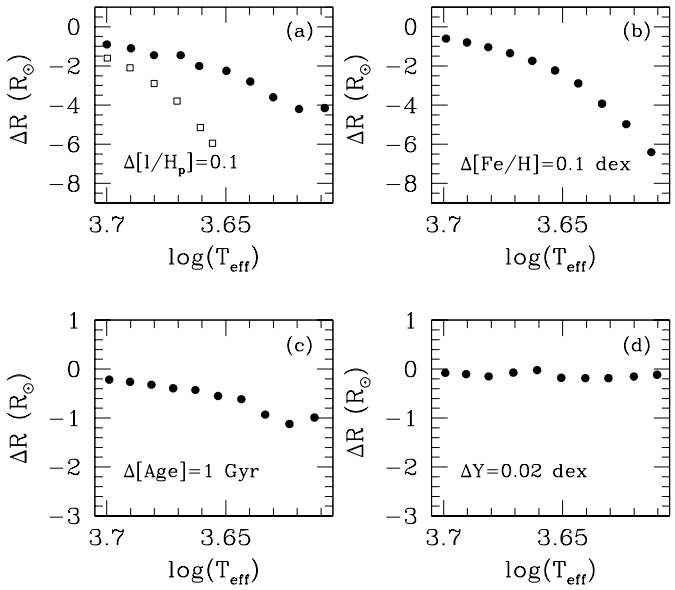

Fig. 5a–d. Mean variation of radii induced by: **a** A change in the mixing-length parameter $(l/H_{\rm p})$ amounting to 0.1 from 1.9 to 1.8 (full points [Fe/H]=–0.6, open points [Fe/H]=–2.3). **b** A change of metallicity of 0.1 dex, computed from theoretical isochrones in the range $-1.3 \geq [Fe/H] \geq -1.6$. **c** A change of age of 1 Gyr, computed from theoretical isochrones of 9–12 Gyr. **d** A change in the abundance of helium of 0.02 dex. (Notice the change of scale in $\Delta(R)$ axis for Figs. **c** and **d**).

the derived distances on the value of the initial helium content and of the mixing length.

The sensitivity of the distances from the $T_{\rm eff}$–R fitting method to the uncertainty on the cluster age can be estimated by computing the mean gradient $\left[\frac{\Delta R}{\Delta t}\right]$ at constant $T_{\rm eff}$, $l/H_{\rm p}$ and chemical composition from the theoretical isochrones. The variation of radius induced by a change of 1 Gyr in age is shown in Fig. 5c. The most appreciable effect is a variation by approximately ± 1 $R_{\odot}$ at the lower edge of the temperature scale (4000-4400 K). This variation corresponds to a mean relative change of radius amounting to 1.5%, and is smaller than typical observational uncertainties in IRFM radii in this range of temperature (5–10%). An estimate of the age of the cluster with an uncertainty of $\pm$ 1-2 Gyr implies an error of the distance modulus amounting to $\pm$0.03-0.07 mag.

The effect of the uncertainties on the clusters [Fe/H] values can be estimated by computing the mean gradient $\left[\frac{\Delta R}{\Delta [Fe/H]}\right]$ keeping fixed all other parameters ($T_{\rm eff}$, age, Y, $l/H_{\rm p}$). The variation of the theoretical radii induced by a change of 0.1 dex in [Fe/H] is shown in Fig. 5b. The effect on the isochrone is a monotonic variation of radius with effective temperature. The amplitude of the effect shows that [Fe/H] is a critical parameter for determining distance by means of the present method. At the lowest temperatures of the RGB the variation becomes comparable with errors on the empirical radii determination. The total internal uncertainty (random plus systematic) on the high resolution spectroscopic [Fe/H] determinations by Carretta & Gratton (1997) is estimated by the authors to be $\sim$0.1 dex. This value which will be used in the application of the method implies an error amounting typically to $\sim$0.12 mag in the distance moduli derived.

The sensitivity to the uncertainty on the value of the initial helium abundance (Y) has been estimated by computing the mean gradient $\left[\frac{\Delta R}{\Delta Y}\right]$ at constant $T_{\rm eff}$, age, $l/H_{\rm p}$ and [Fe/H]. As it is evident from Fig. 5d, the effect of Y is negligible: a variation by 0.01 dex implies $\Delta R \leq 0.5\%$ which in turn implies a variation of 0.005–0.01 mag in the distance modulus. We just mention here that the two classical methods for deriving globular clusters distances, namely MS-fitting and HB-fitting at the RR Lyrae stars region, are more sensitive to the value of Y. As an example, a variation by 0.02 in the initial Y content changes the HB distance modulus by $\simeq$0.08 mag (larger distances for higher helium content), and the MS one by approximately the same amount (larger distances if the MS template has a higher He content than the cluster one).

To finish this section we have to study the influence of the superadiabatic convection calibration on the derived distances from the $T_{\rm eff} - R$ fitting method. The sensitivity of the RGB radii to the value of the mixing-length parameter adopted has been estimated by computing the gradient $\left[\frac{\Delta R}{\Delta (l/H_{\rm p})}\right]$ at constant $T_{\rm eff}$, age, [Fe/H], and Y, for a reprensentative grid of isochrones. The change of radii is around 10-15% when $l/H_{\rm p}$ is varied by 0.1, which implies a sistematic variation of the distance modulus amounting to 0.20–0.30 mag.

This way, $l/H_{\rm p}$ turns out to be the most critical parameter for the application of the present method to derive cluster distances; our technique allows therefore a semi-empirical test of the convection efficiency adopted in the stellar models. The test relies on a basic point: how well a single value of $l/H_{\rm p}$ adopted for the computation of the isochrones reproduces the distance scale obtained via MS- and HB-fitting, methods which are independent on the convective treatment.

3.2. Observational errors

In the previous section we have analized the influence of the isochrones input parameters on the distances derived with the RGB-fitting method. Apart from the uncertainties attached to the theoretical isochrones, we have to take into account also the influence of uncertainties in the assumed metallicity and reddening of each cluster on the empirical values of $T_{\rm eff}$ and R derived by means of the IRFM, which have in turn consequences on the accuracy of the derived distance moduli via the RGB-fitting.

An uncertainty by $\pm$0.1 dex on [Fe/H] implies a variation of effective temperatures and radii determined by means of the IRFM amounting to $\pm$0.15% and 0.5% respectively; in consequence the error on the distance moduli is negligible (about $\pm$ 0.01–0.02 mag).

The adopted cluster reddening has an influence on the bolometric flux and the effective temperature of stars, and therefore on their empirical radii. We have considered a reddening uncertainty amounting to $\pm$0.02 mag, a conservative estimate (based

Table 4. Contributions (in magnitudes) to the total error budget on the distance modulus from RGB stars, considering the individual uncertainties of the input parameters of the fits.

Cluster	Δ(age)=$\pm$ 2 Gyr	Δ[Fe/H]=$\pm$0.1	ΔY=$\pm$0.02	ΔE(B-V)=$\pm$0.02	Δ (fit)
M92	0.06	0.10	0.02	0.07	0.01
M15	0.06	0.11	0.02	0.07	0.04
M68	0.06	0.14	0.01	0.06	0.03
M13	0.06	0.15	0.02	0.06	0.01
M3	0.05	0.14	0.01	0.06	0.01
NGC1261	0.06	0.15	0.01	0.06	0.03
NGC362	0.06	0.13	0.01	0.06	0.02
M5	0.06	0.13	0.02	0.06	0.01
NGC288	0.07	0.13	0.02	0.06	0.01
M71	0.07	0.14	0.01	0.06	0.01
47 Tuc	0.07	0.14	0.01	0.07	0.01
M67	0.07	0.13	0.01	0.06	0.02

Table 5. Distances derived for the clusters in the sample. The parameters adopted in the fits are also given.

Cluster	$[Fe/H]$	Age (Gyr)	$l/H_{\rm p}$	E(B-V)	$D_{\rm RGB}$ (Kpc)	$(m-M)_0$(RGB)	N. of stars
M92	–2.16	13.0	1.8	0.02	11.3	15.27$\pm$0.14	13
M15	–2.12	12.0	1.8	0.10	10.3	15.06$\pm$0.15	5
M68	–2.00	12.0	1.8	0.04	11.5	15.30$\pm$0.17	6
M13	–1.39	10.0	1.8	0.02	7.7	14.43$\pm$0.17	13
M3	–1.34	10.0	1.8	0.01	11.3	15.27$\pm$0.16	34
NGC1261	–1.15	10.9	1.8	0.00	13.8	15.70$\pm$0.18	6
NGC362	–1.15	9.0	1.8	0.06	8.8	14.72$\pm$0.16	21
M5	–1.11	10.0	1.8	0.03	7.6	14.40$\pm$0.16	25
NGC288	–1.07	9.0	1.8	0.04	8.6	14.66$\pm$0.16	14
M71	–0.70	9.0	1.8	0.27	4.5	13.27$\pm$0.17	25
47 Tuc	–0.70	9.0	1.8	0.04	5.2	13.58$\pm$0.17	48
M67	–0.08	3.5	1.8	0.04	0.8	9.50$\pm$0.16	21

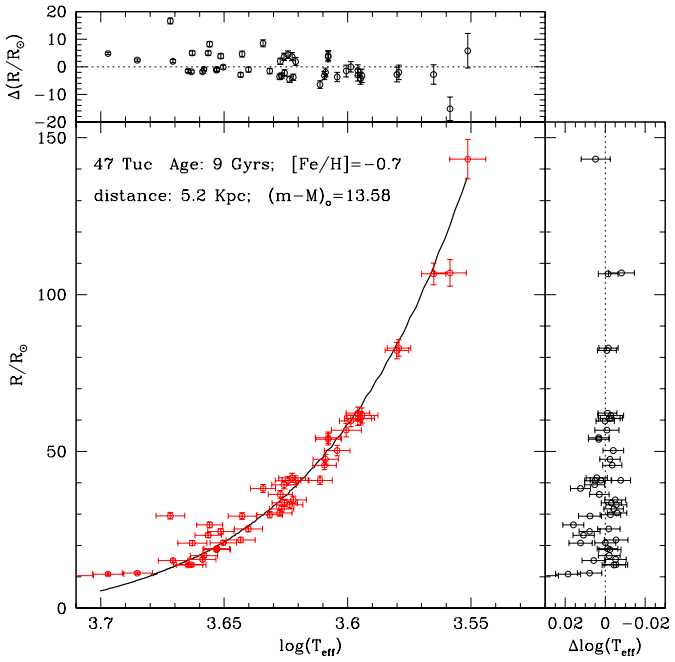

Fig. 6. Fit of 47Tuc giants to the isochrone. Top and right panels show the residuals of the fit in both axis.

on Zinn 1985 results) for the case of the observed clusters, which have almost all of them low reddenings; the resulting error on the clusters distance moduli is approximately 0.06 mag.

3.3. Results: The check of the mixing-length parameter

We have applied our method to the RGB of a selected sample of GCs which cover the range of metallicities observed in our Galaxy: M92, M68, M15, M13, M3, NGC1261, NGC362, M5, NGC288, M71, 47 Tuc, and the old open cluster M67[2]. The theoretical isochrones with parameters adequate to each cluster were selected in order to derive clusters distances by minimising the differences between theoretical and observed ($log(T_{\rm eff})$, R) values using a least squares method. The IRFM temperatures for the giant stars of these clusters have been revised taking into account the slight differences in metallicity and reddening from those adopted in paper I, and computed afresh for M15, M68 and M5. In Table 7, se show temperatures adopted in our analysis, and the final radii obtained for the entire sample of GCs giant stars.

[2] Although this is a galactic cluster the morphology of its RGB resembles that of a globular cluster.

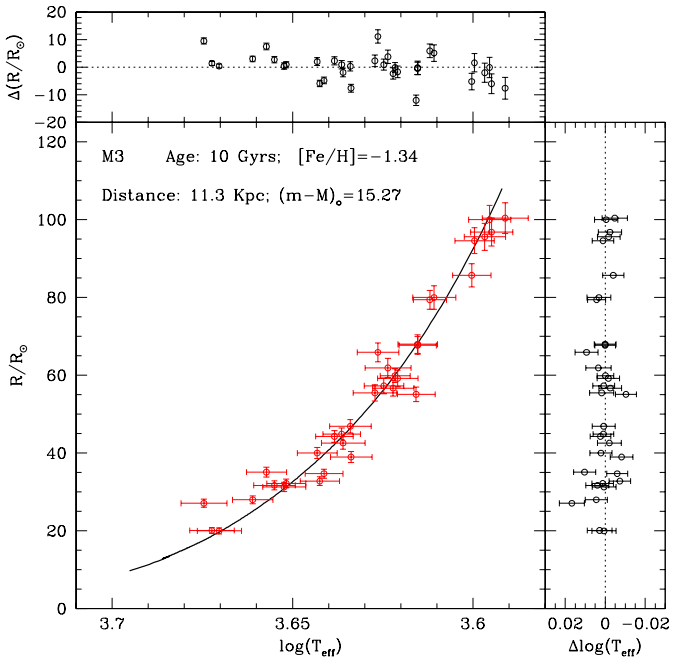

Fig. 7. Fit of M3 giants to the isochrone. Top and right panels show the residuals of the fit in both axis.

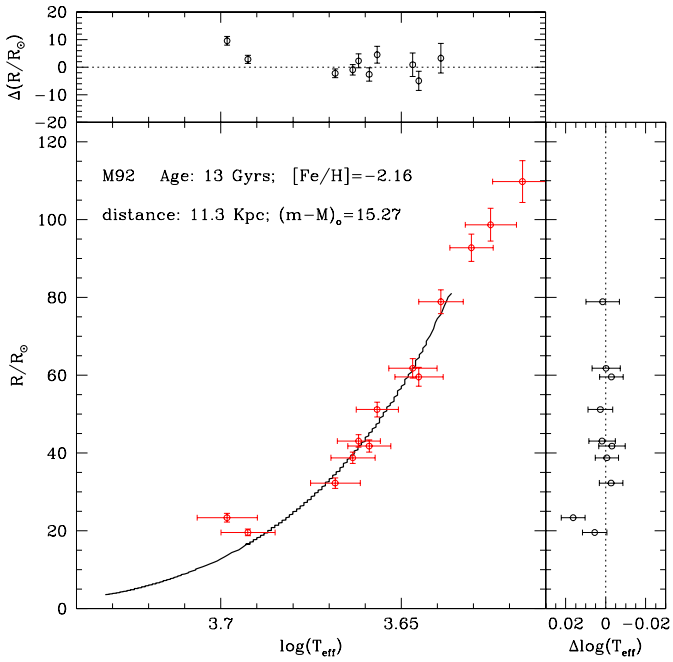

Fig. 8. Fit of M92 giants to the isochrone. Top and right panels show the residuals of the fit in both axis.

Clusters ages were derived using the Salaris & Weiss (1998) models, and are based on the HB distances displayed in Table 6 – derived from Zero Age Horizontal Branch (ZAHB) models homogeneous with the ones we are using for the $T_{\rm eff}$-R fitting – and Carretta & Gratton (1997) GC metallicities, based on high resolution spectroscopic observations of red giants in globular clusters. The errors on the adopted [Fe/H] values are of the order of 0.1 dex.

The observational values for the clusters ZAHB and Turn Off levels come from Buonanno et al. (1998). In the case of M67 the HB distance has been obtained from a fit to the He burning clump region in the observational data by Montgomery et al. (1993), and the age from a fit to the Turn Off position from the same data. Reddenings have been taken from Zinn (1985); all the clusters we have considered (with the exception of M71 and M15) have generally low reddenings, and the error in their determination is of the order of 0.01-0.02 mag. In the case of M67 we adopted the median value among the reddening determinations cited by Chaboyer et al. (1999; E(B-V) in the range 0.02 – 0.06 mag).

In Figs. 6—8 we show a few examples of the fits with the distribution of residuals in both axis. In Table 5, we display the derived distances and distance moduli for our sample of clusters with metallicities ranging from [Fe/H]=0 to [Fe/H]=–2.16. The formal error on the fits, taking into account only the observational errors on the stellar $T_{\rm eff}$ and R values, is small (about $\pm$ 0.02 mag in general). However one must take also into account the sources of errors discussed in the previous sections. We have therefore added in quadrature the contributions due to an uncertainty of $\pm$2 Gyr in the GC ages derived from the Turn Off position, an indetermination by $\pm$0.1 dex on the metallicity, by $\pm$0.02 on the initial Y, and by $\pm$0.02 mag on the clusters reddenings, together with the formal error of the fit. The values of each single contribution to the final error for each individual cluster are given in Table 4, while the total errors appear in Table 5.

In spite of its remoteness, three stars catalogued as members of M67 (NGC2682) have been measured by Hipparcos: NGC2682 81 (HIP 43465) has a parallax of 1.05$\pm$1.96 milliarcseconds, this implies a distance of 950^{+950}_{-627} pc. NGC2682 170 (HIP 43491) has a negative parallax amounting to –1.21$\pm$1.88 milliarcseconds, obviously this value is unuseful to estimate its distance. NGC2682 242 (HIP 43519) has a parallax of 4.42$\pm$1.26 milliarcseconds implying a distance of 226^{+90}_{-50} pc, therefore it is a field star not member of the cluster. Unfortunately, we must conclude that these measurements are not useful to check directly the distances obtained by the $T_{\rm eff} - R$ fitting of RGB stars.

In Table 6, we show the distances obtained from HB-fitting and with the MS-fitting distance scale based on Hipparcos subdwarfs by Carretta et al. (1999). Apparent distance moduli have been converted into dereddened distance moduli by using $A_{\rm V}$=3.1E(B-V). The MS-fitting distances from Carretta et al. (1999) are determined by considering metallicities on the same scale of Carretta & Gratton (1997) used here, and slightly different reddenings. However, the differences are on average less than 0.01 mag, and this does not introduce serious inconsistencies in the comparison with our results. The error bars on the MS-fitting distances (as quoted by Carretta et al. 1999) are given in Table 6 as well; the typical error bar on the HB distances, obtained combining the observational error on the ZAHB level and the uncertainty due to the error on the cluster metallicities is $\simeq$0.12 mag.

Table 6. Distances derived from MS- and HB-fitting for the clusters in the sample.

Cluster	$D_{\rm HB}$ (Kpc)	$(m-M)_0$(HB)	$D_{\rm MS}$ (Kpc)	$(m-M)_0$(MS)
M92	8.7	14.70	8.5	14.64±0.07
M15	11.0	15.21		
M68	11.3	15.26	10.6	15.13±0.06
M13	7.4	14.36	7.5	14.38±0.04
M3	10.5	15.10		
NGC1261	16.8	16.13		
NGC362	8.6	14.67	9.2	14.81±0.05
M5	7.9	14.48	7.8	14.46±0.05
NGC288	8.7	14.69	9.3	14.85±0.05
M71	4.0	13.02		
47 Tuc	4.7	13.38	4.7	13.38±0.09
M67	0.9	9.68		

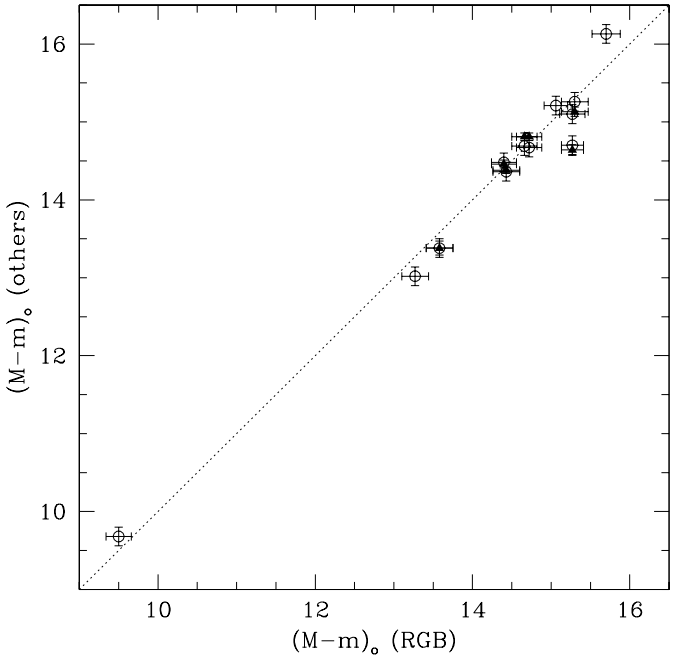

Fig. 9. Comparison between distance moduli derived by RGB-fitting and those obtained by other methods: MS-fitting (triangles), HB-fitting (open circles)

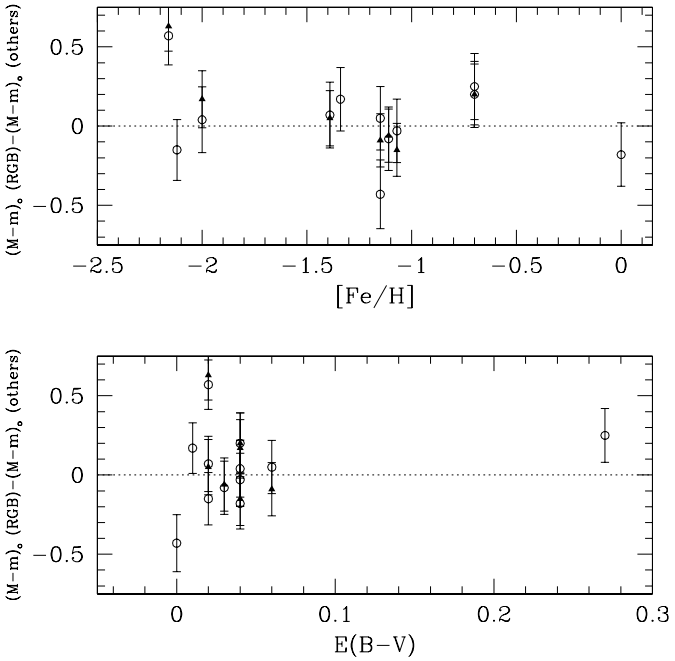

Fig. 10. Differences between distance moduli derived by RGB-fitting and those obtained by other methods: MS-fitting (triangles), HB-fitting (open circles). (top) against metallicity, (bottom) against reddening.

The comparison of the distance scale deduced from the RGB-fitting method with those derived by MS- and HB-fitting shows a conspicuous consistence (Figs. 9 and 10). It is also interesting to notice the very good agreement between the MS-fitting and HB distance scales, as discussed in Salaris & Weiss (1998).

There is however a remarkable exception: M92. As it is evident from Fig. 8, stellar models do not extend enough to cover all the range of $T_{\rm eff}$ and R observational values. Moreover, the derived distance modulus is largely inconsistent with either the MS- or HB-fitting one. Even if the stars with radius larger than the theoretical counterparts are Asymptotic Giant Branch objects, this does not explain the large distance modulus derived. Reasonable uncertainties on the reddening, metallicity and age of the cluster are unable to eliminate the whole discrepancy either. A large decrease of $l/H_{\rm p}$ (by ≈0.2-0.3) would be necessary to enforce agreement with the HB or MS distance moduli, but this is in contradiction with the fact that M68 and M15, the other metal poor clusters in the sample, show a good agreement with theory and a distance modulus consistent with the MS- and HB-fitting. A possible explanation of the discrepancy could be the presence of systematic errors either in the visible photometry on which MS- and HB-fitting are based, or in the near IR photometry on which RGB-fitting is based.

After computing the differences $\Delta(m-M)_0^{\rm MS-RGB}$ between the RGB and MS-fitting distance moduli, we analyzed their correlation with the cluster metallicities. We found that the correlation is significant by less than 2σ if one includes M92, and by less than 1σ if M92 is neglected. An analogous result is found by considering the differences $\Delta(m-M)_0^{\rm HB-RGB}$ be-

Table 7. Effective temperatures derived by means of the IRFM with metallicities and reddenings of Table 5, and derived radii by means of the RGB-fitting. Identifications: M3 numbers from Cohen et al. 1978 and Arribas & Martínez-Roger 1987; M13, M92 and M67 numbers from Cohen et al. 1978; M71 numbers from Frogel et al. 1979; 47 Tuc numbers from Frogel et al. 1981; M15, M68, M5, NGC288, NGC1261, NGC362 numbers from Frogel et al. 1983.

Star	$T_{\rm eff}$ (K)	R ($R_\odot$)	Star	$T_{\rm eff}$ (K)	R ($R_\odot$)	Star	$T_{\rm eff}$ (K)	R ($R_\odot$)	Star	$T_{\rm eff}$ (K)	R ($R_\odot$)
	— M92 —		AM313	4542±58	35.0±1.5	III56	4545±51	29.5±1.0	1603	3802±42	82.0±2.5
III13	4134±80	110±5	AM428	4203±62	62.0±2.5	III78	4090±49	60.0±2.0	1604	4241±48	30.5±1.0
VII18	4219±69	99±4	AM444	4189±55	56.5±2.0	IV3	4807±57	11.5±0.5	2416	4085±46	41.0±1.5
X49	4271±59	93±3	AM464	4128±50	55.0±2.0	IV19	4068±40	61.0±2.0	2426	3943±43	62.0±2.0
III65	4355±62	79±3	AM496	4177±54	59.0±2.0	IV28	4591±53	17.5±0.5	2525	4209±50	40.5±1.5
XII8	4434±68	62±3	AM525	3984±49	85.5±3.0	IV47	4050±50	71.0±2.5	2603	4202±51	33.0±1.0
XI19	4417±68	60±2	AM557	4184±40	60.0±1.5	IV59	4243±45	51.0±1.5	2605	4224±49	39.5±1.5
II70	4536±61	51±2	AM567	4305±57	47.0±1.5	IV81	3963±53	85.5±3.0	3407	4281±51	30.0±1.0
III82	4590±63	43±2	AM586	3934±53	97.0±3.5	IV86	5439±97	8.5±0.5	3410	4367±57	25.5±1.0
IV10	4559±63	42±2	AM605	4390±55	33.0±1.0		— NGC288 —		3501	3969±42	59.5±2.0
IV2	4607±65	39±1	AM617	4081±56	80.0±3.0	C19	4797±64	15.5±0.5	3512	3674±42	106.5±3.5
IV114	4659±74	32±1	AM627	4703±67	20.0±1.0	C20	4085±61	57.0±2.5	4411	4606±63	14.0±0.5
III4	4992±96	23±1	AM650	4329±52	45.0±1.5	C23	4823±62	14.0±0.5	4415	4697±63	29.5±1.0
II12	4926±85	20±1	AM659	4397±56	40.0±1.5	C32	4886±63	10.5±0.5	4417	4978±72	11.0±0.5
	— M15 —		AM675	4214±53	57.5±2.0	C33	4486±60	26.0±1.0	4418	3943±50	60.5±2.0
I12	4182±55	101.0±4		— NGC1261 —		C36	4460±59	28.5±1.0	4503	4308±50	38.0±1.5
II29	4559±43	63.0±2	3	3897±50	73.0±3.0	A77	4246±56	49.0±2.0	4603	4054±48	54.5±2.0
II64	4522±40	56.0±2	9	3916±52	89.0±3.0	A78	4134±46	59.0±2.0	5309	3986±56	57.0±2.0
II75	4291±45	79.0±3	10	3906±51	76.0±3.0	A80	4555±57	27.0±1.0	5312	3933±50	60.5±2.0
S6	4348±47	62.5±2	11	4079±60	49.0±2.0	A96	4048±45	70.0±2.5	5404	4528±55	26.5±1.0
	— M68 —		52	4117±63	57.5±2.5	A194	4293±50	47.5±1.5	5406	4188±51	34.5±1.0
A14	4192±58	83±3	81	4201±56	58.5±2.0	A231	4505±62	32.0±1.5	5422	4068±45	45.5±1.5
I82	4200±58	84±3		— NGC362 —		A245	4397±53	38.0±1.5	5427	4234±48	31.5±1.0
I144	4323±49	70±3	I2	4590±54	23.0±1.0	A260	3772±54	107.0±4.0	5527	4498±54	19.0±0.5
I256	4375±55	72±3	I23	4312±48	41.0±1.5		— M71 —		5529	3795±42	83.0±2.5
I260	4250±52	83±3	I44	4317±47	48.0±1.5	B	3600±72	126.5±6.5	5627	4179±52	41.0±1.5
ZNG2	4420±58	74±3	I52	4590±57	16.0±0.5	A4	3945±68	68.5±3.0	5739	4064±48	47.5±1.5
	— M13 —		II20	4001±53	72.0±2.5	A6	3897±72	66.5±3.0	6407	4393±58	29.5±1.0
I2	4780±73	17.0±1.0	II40	4749±66	16.0±1.0	S	4147±47	39.5±1.5	6408	4222±50	33.5±1.0
I18	4604±63	21.5±1.0	II43	4648±59	28.0±1.0	A9	4036±58	42.5±1.5	6502	5141±95	10.5±0.5
I23	4519±64	32.5±1.5	II47	4773±64	21.0±1.0	N	4840±60	19.0±1.0	6509	4499±58	18.5±0.5
I24	4374±57	42.0±1.5	II49	4447±57	29.0±1.0	A7	4411±53	24.0±1.0	7320	3618±54	107.0±4.5
I48	3929±45	93.0±3.0	III4	4337±48	36.5±1.0	A5	4531±57	20.0±1.0	7502	4558±57	15.5±0.5
II67	3894±45	93.0±3.0	III11	3870±50	97.0±3.5	X	5132±85	10.5±0.5	7507	4686±64	15.0±0.5
II76	4202±52	56.5±2.0	III25	4388±52	37.5±1.5	A3	5159±86	10.0±0.5	8406	4020±48	50.5±2.0
II90	3918±45	86.0±3.0	III37	4340±49	47.5±1.5	C	4856±60	11.5±0.5	8416	4471±55	21.0±1.0
III18	4270±56	48.0±2.0	III39	4015±51	80.5±3.0	A2	4706±62	12.0±0.5	8517	4239±48	36.5±1.0
III56	4013±41	81.0±2.5	III44	4034±49	70.5±2.5	18	4836±62	12.0±0.5	8518	4534±56	23.5±1.0
III63	4067±55	73.5±3.0	III63	3926±48	83.5±3.0	19	5295±94	9.5±0.5		— M67 —	
III73	4164±52	64.0±2.5	III70	4148±47	64.0±2.0	21	4349±48	32.0±1.0	84	4702±61	10.0±0.5
IV25	3792±127	96.0±7.5	IV84	4044±49	63.5±2.0	29	3574±50	146.0±5.5	94	6058±116	2.0±0.5
	— M3 —		IV91	4410±55	38.0±1.5	30	3925±56	76.5±3.0	105	4414±59	14.0±0.5
I21	4124±52	68.0±2.5	IV100	3874±55	85.0±3.5	45	3920±54	66.0±2.5	108	4190±52	22.0±1.0
II18	4727±69	27.0±1.0	V2	3792±50	101.0±4.0	46	3901±54	70.0±2.5	115	5926±109	2.0±0.5
II46	3951±52	95.5±3.5		— M5 —		75	4868±77	10.0±0.5	117	5210±92	3.0±0.5
III28	4092±43	79.5±2.5	I1	5027±67	14.5±0.5	76	4635±57	15.5±0.5	141	4711±61	10.5±0.5
III77	4238±59	55.5±2.0	I4	4350±46	33.0±1.0	77	3935±56	57.0±2.0	151	4760±59	10.0±0.5
IV25	4349±52	44.5±1.5	I14	4193±48	45.0±1.5	78	4333±48	36.0±1.0	164	4654±64	10.5±0.5
193	4681±66	20.0±1.0	I20	4201±47	57.5±2.0	79	4556±56	17.5±1.0	170	4236±48	21.5±1.0
216	4519±60	31.5±1.0	I25	4422±53	28.5±1.0	113	3831±66	70.0±3.0	193	4868±69	4.0±0.5
1937	3939±53	100.0±3.5	I55	4696±61	23.5±1.0		— 47Tuc —		223	4672±63	10.5±0.5
AA	3977±50	94.5±3.5	I61	4325±46	34.0±1.0	1406	4399±60	22.0±1.0	224	4658±65	9.5±0.5
BI	4491±62	31.5±1.0	I67	4923±70	17.0±0.5	1407	4552±58	17.0±0.5	231	4791±62	6.0±0.5
AM26	3900±57	100.5±4.0	I68	4069±51	68.5±2.5	1414	4844±68	11.0±0.5	244	5032±83	7.5±0.5
AM33	4124±49	67.5±2.5	II9	4230±48	60.0±2.0	1421	3559±60	143.0±6.5	I17	4883±69	4.0±0.5
AM46	4485±56	32.0±1.0	II50	4371±48	24.5±1.0	1425	4620±63	14.0±0.5	I22	5009±70	3.0±0.5
AM53	4325±60	42.5±1.5	II51	4522±54	22.0±1.0	1505	3928±58	61.5±2.5	III34	4630±63	7.5±0.5
AM68	4378±53	34.5±1.0	III3	4060±51	70.0±2.5	1510	4054±49	54.0±2.0	IV20	4586±59	8.0±0.5
AM72	4303±57	39.0±1.5	III16	4878±62	16.0±0.5	1513	4193±52	41.5±1.5	IV77	4943±69	3.0±0.5
AM155	4582±59	28.0±1.0	III36	4179±47	51.0±1.5	1518	4481±55	24.5±1.0	IV81	5310±96	2.5±0.5
AM311	4230±56	66.0±2.5	III53	4658±58	25.0±1.0	1602	4602±62	21.0±1.0			

tween the RGB and HB-fitting distance moduli. This fact seems to indicate that there is no significant trend of the difference $\Delta(m-M)_0$ with [Fe/H], and therefore the difference between 'model' and 'real' mixing length has no trend with metallicity. The mean value of $\Delta(m-M)_0^{\rm MS-RGB}$ is small. It amounts to $\Delta(m-M)_0^{\rm MS-RGB} = -0.09\pm0.06$ including M92, and $\Delta(m-M)_0^{\rm MS-RGB} = -0.02\pm0.07$ without this cluster. In the case of $\Delta(m-M)_0^{\rm HB-RGB}$ we find $\Delta(m-M)_0^{\rm HB-RGB} = -0.04\pm0.06$ considering all clusters, and $\Delta(m-M)_0^{\rm HB-RGB} = -0.003\pm0.06$ when excluding M92. By considering the sensitivity of the clusters distance moduli to the value of $(l/H_{\rm p})$ (Sect. 3.1), these figures imply that the difference between the mixing length parameter used in the stellar models and the 'real' one suggested by observations, (when using the Carretta & Gratton 1997 metallicities and the Hipparcos subdwarfs MS-fitting distance scale, or the HB distance scale from Salaris & Weiss 1998), is consistent with zero, and in any case less than 0.1.

The present discussion illustrates the utility of the $T_{\rm eff}$-R distances for testing the efficiency of superadiabatic convection in RGB envelopes, irrespective of the convection formalism used. In the case of the models we employed, the solar value of the mixing length parameter appears adequate to derive also the superadiabatic gradient in the envelope of RGB stars over a wide range of metallicities. However, it is important to be aware of the fact that the number of data for the very metal-poor clusters is small. In particular, if we neglect M92 for the reasons previously discussed, the convection calibration at the lower end of the GC metallicities rests on only eleven stars observed in M68 and M15. More observations of metal-poor cluster giants are therefore needed.

4. Summary and conclusions

We have applied recent determinations of effective temperatures and bolometric fluxes of giant stars to the analysis of several points connected with stellar structure and evolution problems. The results are summarized in the following points:

(1) We have showed the observational consistence of IRFM diameters with those directly measured by means of interferometric techniques.

(2) Based on the average values obtained for a sample of approximately 300 giant stars, we present semi-empirically determined relations between $T_{\rm eff}$ and linear radii, based upon the IRFM and Hipparcos parallaxes. For the first time, this kind of relations is extended to population II giants.
The comparison of the semi-empirical mean relations $T_{\rm eff}-R$ with theoretical isochrones shows, in general, a good agreement, however minor discrepancies are noticed which could require further analysis.

(3) We have devised a method to derive distance moduli of stellar clusters which nicely complement those usually employed, and serves to test the consistency of convection theories adopted in stellar models.
If R, $T_{\rm eff}$ and metal abundance of a sample of RGB stars in a cluster are known and the distance scale is fixed, the value of the mixing–length parameter $l/H_{\rm p}$ can be estimated, and tests for different convection theories can be performed avoiding the use of colour$-T_{\rm eff}$ transformations. In applying the method to Salaris & Weiss (1998) isochrones, we find that the value of $l/H_{\rm p}$ used is fairly consistent with the observations when either HB-fitting distances, or the Hipparcos MS-fitting distance scale are adopted.
In connection with this point, our analysis shows clearly how the advent of high quality near-IR array photometry can help in testing the convection calibration with the method presently devised.

Acknowledgements. We are grateful to Dr. E. Masana for valuable comments. We are also grateful to the referee Dr. F. Keenan for his swift and precise assessment of the paper.

References

Alexander D.R., Ferguson J.W., 1994, ApJ 437, 879
Alonso A., Arribas S., Martínez-Roger C., 1994, A&A 284, 684
Alonso A., Arribas S., Martínez-Roger C., 1999, A&AS 139, 335 (Paper I)
Arribas S., Martínez-Roger C., 1987, A&A 178, 107
Baschek B., Scholz M., Wehrse R., 1991, A&A 246, 374
Blackwell D.E., Petford A.D., Arribas S., Haddock D.J., Selby M.J. 1990, A&A 232, 396
Böhm-Vitense E., 1958, Zs Ap. 46, 108
Buonanno R., Corsi C.E., Pulone L., Fusi Pecci F., Bellazzini M., 1998, A&A 333, 505
Canuto V., Goldman I., Mazzitelli I., 1996, ApJ 473, 550
Carretta E., Gratton R.G., 1997, A&AS 121, 95
Carretta E., Gratton R.G., Clementini G., Fusi-Pecci F., 1999, ApJS in press
Chaboyer B., Green E.M., Liebert J., 1999, AJ 117, 1360
Cohen J.G., Frogel J.A., Persson S.E., 1978, ApJ 222, 165
Cox J.P., Giuli R.T., 1968, Principles of Stellar Structure. Vol. 1 Gordon & Breach, New York
Di Benedetto G.P., Rabbia Y., 1987, A&A 188, 114
Dick H.M., van Belle G.T., Thompson R.R., 1998, AJ 116, 981
ESA,, 1997, The Hipparcos and Tycho Catalogues. ESA SP-1200
Freytag B., Salaris M., 1999, ApJ 513, L49
Frogel J.A., Persson S.E., Cohen J.G., 1979, ApJ 227, 499
Frogel J.A., Persson S.E., Cohen J.G., 1981, ApJ 246, 842
Frogel J.A., Persson S.E., Cohen J.G., 1983, ApJS 53, 713
Hutter D.J., Johnston K.J., Mozurkewich D., et al., 1989, ApJ 340, 1103
Iglesias C.A., Rogers F.J., 1996, ApJ 464, 943
Krishna-Swamy K.S., 1966, ApJ 145, 174
Ludwig H.G., Freytag B., Steffen M., 1999, A&A 346, 111
Mazzitelli I., D'Antona F., Caloi V., 1995, A&A 302, 382
Montgomery K.A., Marschall L.A., Janes K.A., 1993, AJ 106, 181
Mozurkewich D., Johnston K.J., Simon R.S., et al., 1991, AJ 101, 2207
Pagel B.E.J., Portinari L., 1998, MNRAS 298, 747
Perrin G., Coudé du Foresto V., Ridgway S.T., et al., 1998, A&A 331, 619
Ridgway S.T., Joyce R.R., White N.M., Wing R.F., 1980, ApJ 235, 126
Rogers F.J., Swenson F.J., Iglesias C.A., 1996, ApJ 456, 902
Salaris M., Cassisi S., 1996, A&A 305, 858
Salaris M., Weiss A., 1998, A&A 335, 943
Sandage A., 1986, ARA&A 24, 421
van Belle G.T., Lane B.F., Thompson R.R., et al., 1999, AJ 117, 521
Weiss A., Salaris M., 1999, A&A 346, 897
Zinn R., 1985, ApJ 293, 424